12th International Symposium on Turbulence and Shear Flow Phenomena (TSFP12)
Osaka, Japan (Online), July 19-22, 2022

ULTRA-FINE ROUGHNESS EFFECT ON TRANSITION DELAY USING DIRECT NUMERICAL SIMULATION

Shingo Hamada
Department of Aerospace Engineering,
Tohoku University
6-6 Aramaki Aza Aoba, Aoba-ku,
Sendai, Miyagi 980-8579, Japan
shingo.hamada.s5@dc.thoku.ac.jp

Aiko Yakeno
Institutute of Fluid Science,
Tohoku University
2-1-1 Katahira, Aoba-ku,
Sendai, Miyagi 980-8577, Japan
aiko.yakeno.b4@dc.tohoku.ac.jp

Shigeru Obayashi
Institutute of Fluid Science,
Tohoku University
2-1-1 Katahira, Aoba-ku,
Sendai, Miyagi 980-8577, Japan
s.obayashi@tohoku.ac.jp

ABSTRACT

Direct numerical simulations (DNSs) were conducted to analyze the effect of a fine sand-grind rough surface on a laminar-turbulent transition. While wall roughness has often been discussed to increase drag in a turbulent flow state, this study focuses on its drag reduction effect. We applied the Volume Penalization Method (VPM) and zonal method to resolve the ultra-fine sand-grind rough surface on a flatplate, in the three-dimensional DNSs. We confirmed the Tollmien-Schlichting (T-S) wave transition phenomena has been modified on the sand-grind rough surface. T-S wave on the rough surface broke down to the three-dimensional flow structure the fastest among tested cases, but the turbulent kinetic energy was kept small the most.

INTRODUCTION

The demand for aircraft transportation is increasing, and the demand for CO_2 emission reduction is becoming more and more stringent. There is a need to improve fuel efficiency in ways such as drag reduction. The most significant aerodynamic drag acting on an aircraft is a frictional drag. To reduce this, laminar flow control is used to maintain the laminar flow state longer, and turbulence control is used to reduce frictional drag in a turbulent flow state. Riblets, which are micro-grooves that imitate shark skin, have been studied for many years and have been shown to reduce friction drag by approximately 8% (Walsh *et al.* (1989); Walsh (1992)). However, there are some problems in practical application, such as the maintenance cost for contamination and the fact that the riblets lose their effects if they are not parallel to the streamwise direction.

The possibility of reducing friction drag on rough surfaces with the finer roughness has been referred to by Tani (Tani (1988)), which height is below the viscous sublayer ($Re_k < 6$). Such small roughness has been considered negligible from a flow dynamical aspect. Oguri & Kohama (1996) conducted wind tunnel experiments with the micron-sized distributed roughness, which is under $9[\mu\mathrm{m}]$, that was below the viscous sublayer in a turbulent state. A reduction in frictional drag and turbulent fluctuation intensity of up to $1.9[\%]$ were achieved. The detailed mechanism of the drag reduction has not been clarified. We believe that is based on a different mechanism from that of Riblets, which is based on the suppression of spanwise velocity fluctuations and letting streamwise vortices away from a wall surface. In addition, the use of a micron-sized fiber surface has been also observed to be effective for the transition delay (Kikuchi *et al.* (2004)). Here, we call them the Distributed Micro Roughness (DMR) for a drag reduction.

Tameike *et al.* investigated the effect of a small wavy roughness on the natural transition using two-dimensional direct numerical simulations (DNSs) Tameike *et al.* (2021). It was confirmed that the small wavy roughness kept the Tollmien-Schlichting (T-S) vortices small downstream delaying a transition at a specific roughness wavelength. Recently, the phenomenon has been confirmed by the three-dimensional simulations by using an artificial disturbance to cause a T-S wave upstream Hamada *et al.* (2020). In this study, as the second step, we analyze the flow of the more practical and complicated roughness, such as a sand-grind roughness as tested in experiments.

Though effects of sand-grind roughness in a channel have been investigated experimentally and numerically (Nugroho *et al.* (2021); Jelly & Busse (2019); Kuwata & Nagura (2020)), most of the studies are concerned with the effects in a fully-developed turbulent flow and the increase of friction drag. Their roughness heights are normally higher than the viscous sublayer, and there are few studies on its use for transition delay and turbulent frictional drag reduction.

Therefore, the purpose of this study is to clarify the effect of such ultra-fine distributed roughness, which effect has been referred to and confirmed in experiments to delay the transition and reduce turbulent drag (Tani (1988); Oguri & Kohama (1996); Kikuchi *et al.* (2004)). In this study, we analyze the ef-

fect of sand-grind rough surfaces on a laminar-turbulent transition via the T-S wave on a flatplate.

METHODS

Computational Setup

In this study, we demonstrate the T-S wave transition on a flatplate numerically, by using the in-house LU-ADI three-dimensional compressible Navier-Stokes solver (originally Fujii & Obayashi (1987)). A sixth-order accurate compact scheme is used for the spatial discretization (Lele (1992)), and the three-step TVD Runge-Kutta method is used for time integration (Chi-Wang & Osher (1988)). The simulation schemes are the same as Tameike *et al.* used in their study (Tameike *et al.* (2021)).

The Reynolds number based on the boundary layer thickness δ_s at the inlet boundary is set to 3535. The Mach number is set to 0.2 to obtain sufficiently large time increments within which compressibility effects can be neglected.

The boundary conditions are shown in Figure 1. The time-mean velocity distributions at the inlet boundary are given by the Blausis solution. At the inlet boundary, an artificial disturbance is added in the wall-normal velocity to induce a T-S wave. The periodic condition is applied at the spanwise boundaries. The velocity and pressure are set as free at the outlet boundary. At the far boundary in the wall-normal direction, the pressure and the streamwise velocity are fixed, and the wall-normal and spanwise velocities are set as free.

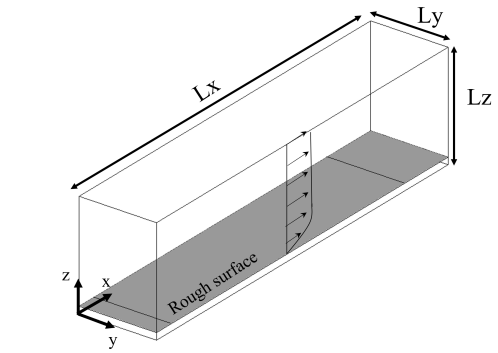

Figure 1. Schematic of the geometry.

Volume Penalization Method

In this study, the Volume Penalization Method (VPM) is used to simulate a three-dimensional rough surface (Liu & Vasilyev (2007), Komatsu *et al.* (2016)). The VP method for compressible flow was proposed by Liu and Vasilyev, and the no-slip condition can be given by adding a penalty term to the Navier-Stokes equations. The VP method can be used to analyze walls of arbitrary geometry without the need to generate a grid fitted to a solid wall.

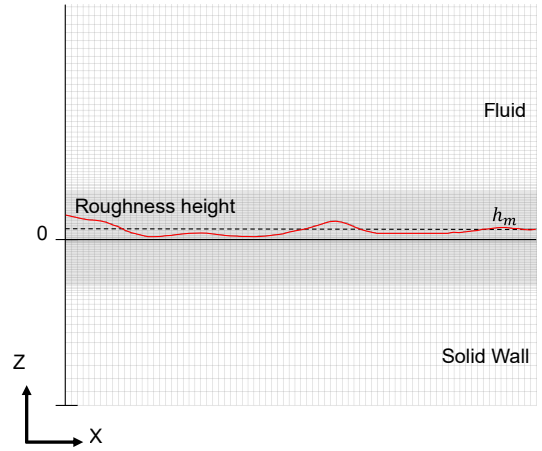

Figure 2. Mask function shape and Grid resolution near the wall.

$$\frac{\partial \rho}{\partial t} + \frac{\partial (\rho u_j)}{\partial x_j} = -\left(\frac{1}{\phi} - 1\right) \chi \frac{\partial (\rho u_j)}{\partial x_j}, \tag{1}$$

$$\frac{\partial (\rho u_j)}{\partial t} + \frac{\partial (\rho u_i u_j)}{\partial x_j} = -\frac{\partial p}{\partial x_i} + \frac{\partial \tau_{ij}}{\partial x_j} - \frac{\chi}{\eta}(u_i - U_{0,i}), \tag{2}$$

$$\frac{\partial e}{\partial t} + \frac{\partial}{\partial x_j}\left[(e+p)u_j\right] = \frac{\partial (u_i \tau_{ij})}{\partial x_j} + \frac{\partial}{\partial x_j}\left(\kappa \frac{\partial T}{\partial x_j}\right) - \frac{\chi}{\eta_T}(T - T_0), \tag{3}$$

where ρ is the density of the fluid, u_i is the flow velocity $U_{0,i}$ is the solid wall velocity and defined as 0. ϕ is porosity and is set to 1. κ is the thermal conductivity. τ_{ij} is the viscous stress tensor. ν is the permeability and is taken to be sufficiently small. The ν_T is the thermal permeability and is assumed to be the same as ν. e is the total energy, p is the pressure, T is the temperature, and T_0 is the solid wall temperature. Since temperature change is negligible in this study, the solid wall temperature is assumed to be the same as the mainstream. The difference in the temperature boundary condition is not expected to be apparent for low Mach number flows, as in this study. Since χ is a mask function and the VP method does not require the generation of a body-fitted grid, an arbitrary shape of a solid wall can be reproduced by defining a mask function.

$$\chi(x) = \begin{cases} 1 \ \text{(Rigidwall)} \\ 0 \ \text{(Fluid)} \end{cases} \tag{4}$$

As shown in Figure 2, near the surface roughness, the roughness is resolved with a sufficient number of grid points in both streamwise direction and wall-normal direction. The resolution is approximately 20 points or more per wavelength of roughness. The VPM is offset from the wall-normal origin and the edges of the computational grid to allow for the number of grid points inside the wall. The VPM tends to accelerate the transition slightly, possibly because the surface profile is simulated by an orthogonal mesh, which is more liable to generate tiny disturbances from the curved surface.

Zonal Method

To reproduce the shape of a rough surface by an orthogonal mesh, sufficient mesh resolution is required. However, a fine mesh width over the entire computational domain would require a huge computational cost. Therefore, in this study, a nested grid was used to capture turbulence with high accuracy while minimizing the computational cost. Two zonal grid distributions are shown in Figure 3.

In the small zone (red), the grid resolution in the streamwise direction is doubled; the small zone has a viscosity scale of $Lz^+ \approx 50$ in the height direction, which captures the viscous sublayer. Global zone (black) has $(N_x, N_y, N_z) = (1454, 151, 284)$ and the computational domain lengths are $(Lx, Ly, Lz) = (56.6, 11.3, 28.3)$ for global zone.

The small zone has $(N_x, N_y, N_z) = (2843, 201, 137)$, and the computational domain lengths are $(L_x, L_y, L_z) = (50.9, 11.3, 0.59)$. However, $N_y = 201$ and $L_y = 14.1$ in the spanwise direction were used for the smooth surface and the two-dimensional wavy rough surface as a comparison. For the calculation of sand-grind rough surfaces, $L_y = 11.3$ was used to keep the computational domain in the span direction as small as possible, since the higher resolution is needed to reproduce the fine irregularities of the rough surfaces.

Sand-grind roughness shape

The effective slope (ES) and skewness coefficient (Sk) of the present sand-grind roughness are calculated based on the following equations (Eq. (5) and Eq. (6)). They are summarised in Table 1.

$$ES = \frac{1}{L_x L_z} \int_x \int_z \left| \frac{\partial h(x,z)}{\partial x} \right| dxdz. \tag{5}$$

$$Sk = \frac{1}{h_{rms}^3 L_x L_z} \int_x \int_z (h(x,z) - h_m)^3 \, dxdz. \tag{6}$$

As mentioned above, the effect of roughness in developed turbulent flows can be clarified to some extent by the skewness and effective slope. The skewness Sk is the bias between the peaks and valleys of the roughness surface. The effective slope ES is the ratio of the roughness height to the roughness interval. In this study, skewness $Sk = 0.395$ and effective slope $ES = 0.125$. This parameter is included in the range of the analysis by Kuwata & Nagura (2020) et al. This value of $Sk = 0.5$ is close to that of $ES = 0.1$, and a downward shift ($\Delta U^+ = 3 \sim 4$) in the mean velocity distribution is confirmed. Furthermore, when ES is relatively small, the difference in ΔU^+ by the value of Sk is reported to be small, suggesting that the difference of Sk in this study is not so important.

The mean height of the sand-grind roughness, h_m, is 0.092 to reproduce the sand-grind on a scale completely corresponding to that of our wind tunnel experiment Suzuki (2021). Based on the roughness height, a single sand-grind roughness data set is not sufficient to cover the full computational domain, so a repeating pattern was used as shown in Figure 4. The repeated boundaries of the rough surfaces were connected smoothly. Although the viscosity unit cannot be strictly determined in the transition process, the viscosity scale is calculated from the flow downstream, which is converted to the viscosity scale to give an average height of $h_m^+ = 15.5$.

Table 1. parameters of rough surfaces.

Sk	ES	h_m	h_{rms}
0.395	0.125	0.092	0.028

RESULTS and DISCUSSION

Turbulent kinetic energy

We show a visualization of the iso-surfaces of the second invariant of the velocity gradient tensor in the instantaneous field of the three-dimensional simulation with a sand-grind surface in Figure 5. The flow structure around each roughness seems to be sufficiently resolved by the present simulation. We compare the difference in turbulent kinetic energy (TKE) in the turbulent transition among the two-dimensional wavy surface, the sand-grind rough surface, and a smooth surface. Figure 6 shows the difference in the spanwise and time-averaged turbulent kinetic energy (TKE, $\overline{u_i' u_i'}$) in x-z plane, (a) sand-grind roughness, (b) wavy roughness (VP method), (c) wavy roughness (Body Fitted grid) and (d) flat plate. And, figure 7 shows the maximum TKE in each wall-normal directions. It was found that the sand-grind rough surface suppressed TKE the most.

Instantaneous flow

The instantaneous snapshots of the three flow fields for one period of the T-S wave are shown in Figure 8. This represents how the T-S roll vortex is induced at the inlet boundary and propagates in the streamwise direction, and eventually breaks to become the three-dimensional structure. Comparing the location of the roll vortex breaks down, the sand-grind rough surface is the fastest among the three cases.

Phase-averaged decomposition

We apply the phase-averaged decomposition to clarify a difference in the transition process, based on the T-S wave period. The turbulent kinetic energy k' is divided into the T-S wave component $\tilde{k}$ and the three-dimensional component k', as shown in the following equation.

$$k = \bar{k} + k', \tag{7}$$

$$k = \bar{k} + \tilde{k} + k''. \tag{8}$$

Comparing the turbulent kinetic energy k on the three rough surfaces, that on a sand-grind surface has kept small downstream the most (Figure 9, 10). From the decomposition statistics, the sand-grind roughness decreases the T-S wave kinetic energy more than the other two surfaces, although it increases the three-dimensional kinetic energy the most upstream but downstream.

In the instantaneous visualization, three-dimensionalization occurs fastest on the sand-grind surface. However, that break seems to make the T-S motion weaken, which results in the total TKE being small downstream.

The T-S kinetic energy was also suppressed on the wavy rough surface, however, the TKE was larger than that of the sand-grind rough surface. That is because of eddies generated at the crests of the wavefronts.

CONCLUSION

In this study, the effect of a sand-grind rough surface on the laminar-turbulent transition was investigated using the

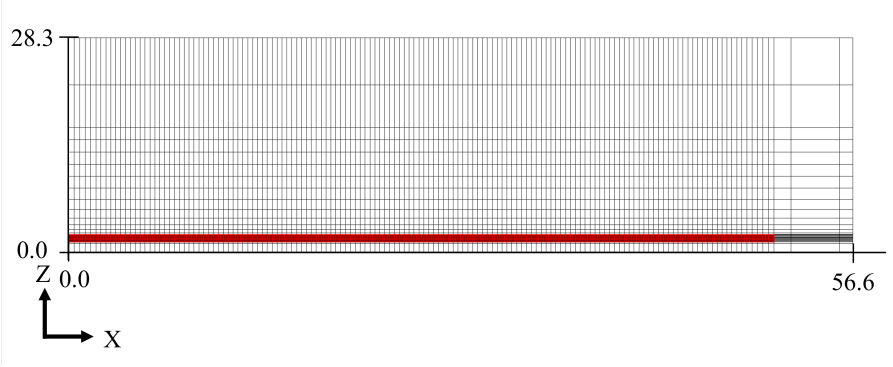

Figure 3. Zonal grid distribution for wall turbulence simulation.

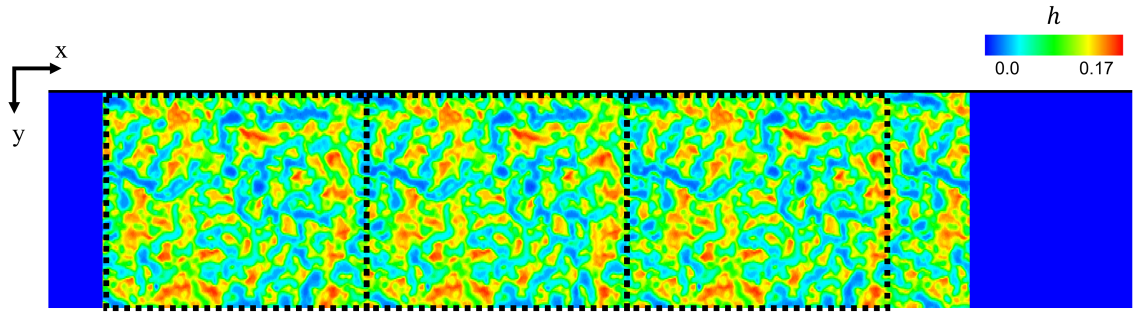

Figure 4. Geometry of the rough surface. The dashed line indicates a single unit tile.

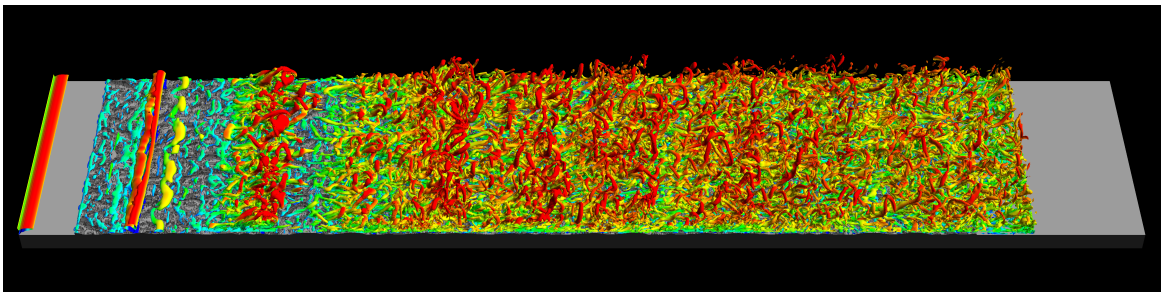

Figure 5. Instantaneous iso-surfaces of the second invariant of velocity gradient tensor; $Q = 0.001$ colored by the streamwise velocity u in the x-y plane.

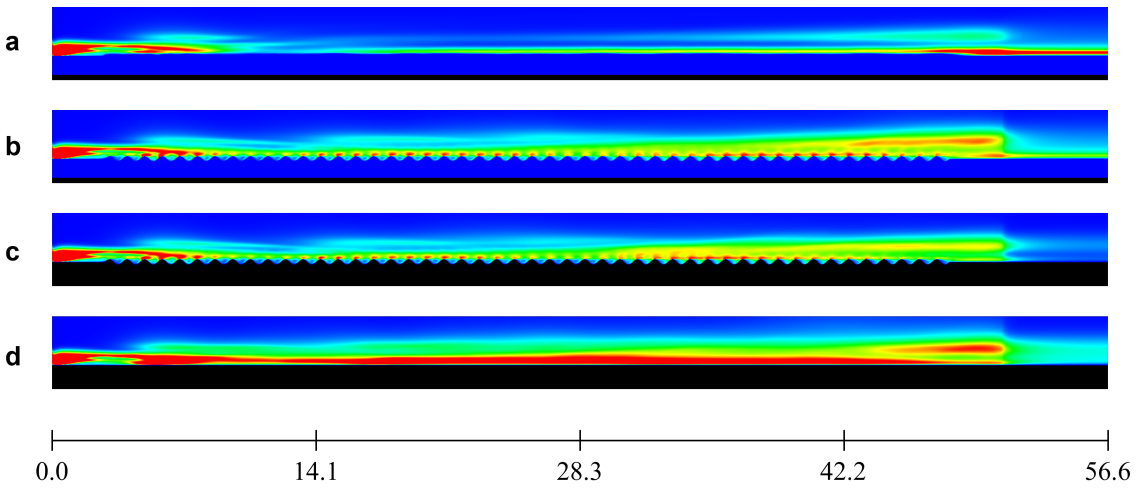

Figure 6. The comparison of turbulent kinetic energy. (a) sand-grind roughness, (b) wavy roughness (VP method), (c) wavy roughness (Body Fitted grid) and (d) flat plate.

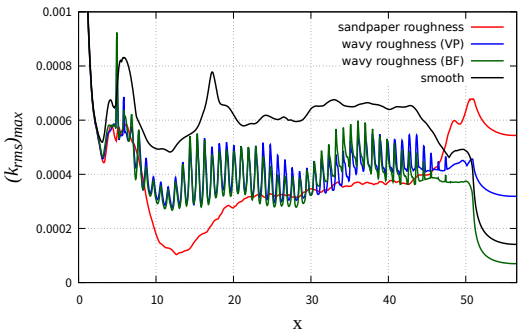

Figure 7. The maximum value of the turbulent kinetic energy k along the x directon

VPM and zonal method in the direct numreical simulations. The two key conclusions were obtained: first, the T-S wave was weakened on two roughness surfaces, not only the wavy rough surface, but also the more complicated random sand-grind rough surface. Second, the breaking up of the T-S wave was promoted on the sand-grind rough surface, but the total turbulent kinetic energy was suppressed the most among tested cases.

ACKNOWLEDGMENTS

Numerical simulations were performed on the "AFI-NITY" supercomputer system at the Advanced Fluid Information Research Center, Institute of Fluid Science, Tohoku University. This research is partially based on a project commissioned by the New Energy and Industrial Technology Development Organization (NEDO) of Japan.

REFERENCES

Chi-Wang, S. & Osher, S. 1988 Efficient implementation of essentially non-oscillatory shock-capturing schemes. *Journal of Computational Physics* **77** (2), 439–471.

Fujii, K. & Obayashi, S. 1987 Navier-stokes simulations of transonic flows over a practical wing configuration. *AIAA Journal* **25** (3), 369–370.

Hamada, S., Yakeno, A., Obayashi, S. & Nugroho, B. 2020 Small wavy roughness effect on ts wave and three-dimensional transition by direct numerical simulation. , vol. 65. APS.

Jelly, T. & Busse, A. 2019 Reynolds number dependence of reynolds and dispersive stresses in turbulent channel flow past irregular near-gaussian roughness. *International Journal of Heat and Fluid Flow* **80**, 108485.

Kikuchi, S., Shimoji, M., Watanabe, H. & Kohama, Y. 2004 Control of bypass transition for textile surface. *JSME International Journal Series B Fluids and Thermal Engineering* **47** (4), 777–785.

Komatsu, R., Iwakami, W. & Hattori, Y. 2016 Direct numerical simulation of aeroacoustic sound by volume penalization method. *Computers & Fluids* **130**, 24–36.

Kuwata, Y. & Nagura, R. 2020 Direct numerical simulation on the effects of surface slope and skewness on rough-wall turbulence. *Physics of Fluids* **32** (10), 105113.

Lele, S.K. 1992 Compact finite difference schemes with spectral-like resolution. *Journal of Computational Physics* **103** (1), 16–42.

Liu, Q. & Vasilyev, O.V. 2007 A brinkman penalization method for compressible flows in complex geometries. *Journal of Computational Physics* **227** (2), 946–966.

Nugroho, B., Monty, JP, Utama, IKAP, Ganapathisubramani, Bharathram & Hutchins, Nicholas 2021 Non–type behaviour of roughness when in-plane wavelength approaches the boundary layer thickness. *Journal of Fluid Mechanics* **911**.

Oguri, E. & Kohama, Y. 1996 Drag reduction by micro-sized distributed surface geometry on a flat plate. *Transactions of the JSME (in Japanese),* **62** (597), 1754–1761.

Suzuki, S. 2021 Effect of wall roughness on wall turbulence by using wind tunnel experiments (in japanese).

Tameike, H., Yakeno, A. & Shigeru, O. 2021 Influence of small wavy roughness on flatplate boundary layer natural transition. *Journal of Fluid Science and Technology* **16** (1), JFST0008–JFST0008.

Tani, I. 1988 Drag reduction by riblet viewed as roughness problem. *Proceedings of the Japan Academy, Series B* **64** (2), 21–24.

Walsh, M. J. 1992 Drag characteristics of v-groove and transverse curvature riblets. *AIAA Journal* **30** (4), 1119–1122.

Walsh, M. J., Sellers, W. L. & McGinley, C. B. 1989 Riblet drag at flight conditions. *Journal of Aircraft* **26** (6), 570–575.

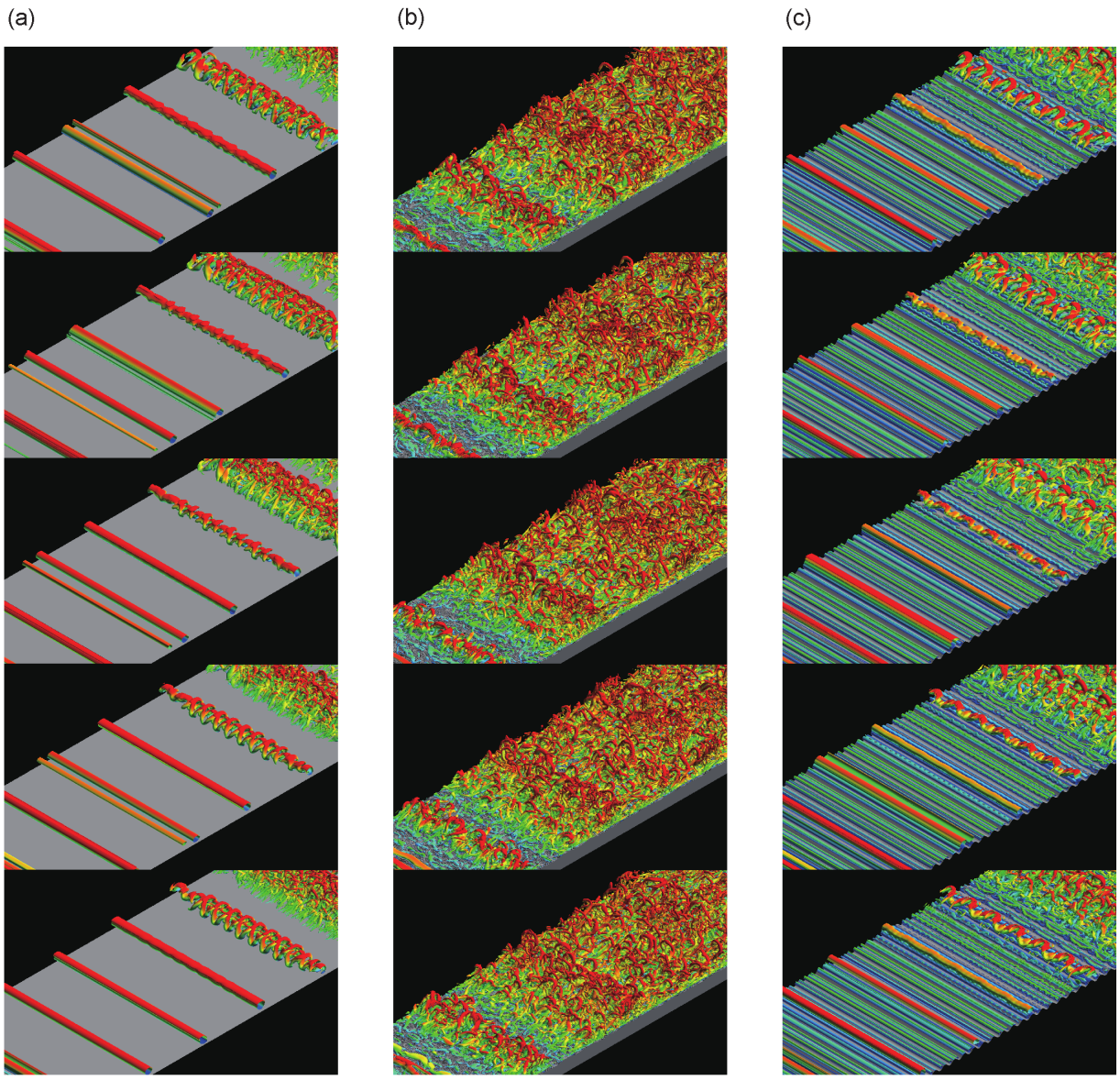

Figure 8. Instantaneous flow fileds: (a)flat plate (b)sand-grind roughness (c)wavy roughness. The isosurface is the second invariant of the velocity gradient tensor $Q = 0.001$ with countour color u from 0.0 to 0.2.

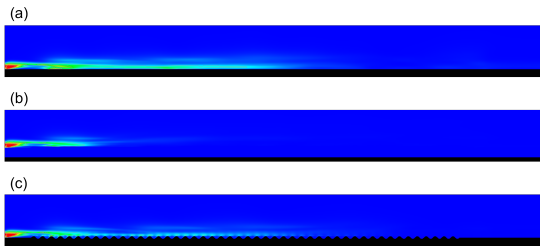

Figure 9. The contour maps of phase-, tiem-andspanwise-averaged turbulent kinetic energy. The T-S wave component. (a) smooth surface, (b) sand-grind roughness, (c) wavy roughness.

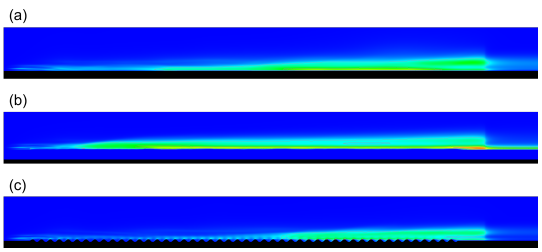

Figure 10. The contour maps of phase-, tiem-andspanwise-averaged turbulent kinetic energy. The three-dimensional component. (a) smooth surface, (b) sand-grind roughness, (c) wavy roughness.